Infrared metafilms on a dielectric substrate

Boubacar Kanté,* Jean-Michel Lourtioz,† and André de Lustrac
Institut d'Electronique Fondamentale, Université Paris-Sud 11, UMR 8622 CNRS, Orsay F-91405, France
(Received 21 August 2009; revised manuscript received 1 October 2009; published 25 November 2009)

Using interferometric measurements and theoretical calculations, we show that a refractive index can be appropriately assigned to a thin plasmonic metafilm on a high-permittivity dielectric. A full analysis in amplitude and in phase of the composite metafilm made of metallic nanoresonators and wires is reported around the first plasmonic resonance. It reveals that contrary to solely intensity measurements, the phase behavior of the air/metafilm/dielectric system dramatically depends on both the damping effects and the dielectric index. A simple model is derived which can apply to various situations in plasmonics and optical metamaterials.

DOI: 10.1103/PhysRevB.80.205120 PACS number(s): 42.70.Qs

There is a growing interest in artificially structured metal-dielectric materials, or metamaterials, for the infrared and visible domains. Fabrication technologies in these domains are for the most part based on thin-film processes including (multi)layer deposition on a substrate, lithography, and etching steps.[1–5] As far as elementary motifs are much smaller than the working wavelength, optical metamaterials can be reasonably described in terms of effective electromagnetic parameters. However, there are several difficulties of either experimental or fundamental nature to retrieve these parameters from thin-film measurements. In principle, the dielectric permittivity ε and magnetic permeability μ can be obtained from the transmittance and reflectance of a single layer provided that interferometric techniques are used to simultaneously measure the phase and amplitude of transmission and reflection coefficients.[6–8] This is not the current procedure used so far in the majority of works, where the optical-phase information is obtained from a numerical model after fitting the model to transmission/reflection spectra measured in intensity.[1,3,4] Another difficulty is due to the fact that the deposited metalayer(s) may possess two different interfaces (inherent asymmetry), for instance, one with air and the other with a dielectric substrate. The effect of a substrate on localized plasmon resonance has been previously investigated for metallic nanoparticles.[9,10] It is now well known that adjacent dielectrics redshift the resonances compared to particles in free space due to the screening of electromagnetic field. The quantification of the shift however depends on the particle shape as well as the polarization of incident light. These experimental investigations were also restricted to intensity measurements. Finally, even in the ideal case of metalayers with symmetrized interfaces, the existence of high-order Bloch modes associated to the periodic arrangement of elementary motifs may have a non-negligible influence on the electromagnetic response of a metalayer stack. This again may violate the retrieval algorithm which is applied to a single layer to derive an effective refractive index for the metalayer stack.[11]

From previous remarks, it is worthwhile noticing that despite an abundant literature on the effective parameters of optical metamaterials, the question remains whether or not the optical response of a single metafilm deposited on a dielectric substrate can be fully interpreted within the effective-index approach. There is a dramatic lack of experiments on this point. In this paper, we analyze both experimentally and theoretically the optical properties of a single metallic metafilm on a dielectric substrate. The metafilm is formed of gold nanowires and split ring resonators (SRRs). By exploiting the interferogram of the asymmetric cavity formed by the metafilm and the substrate, we show that an effective index of refraction can be indeed assigned to the metafilm around the first plasmonic resonance of SRRs (the so-called *LC* resonance). An analysis of the evolution of cavity fringes with frequency reveals the critical influence of the damping frequency associated to plasmonic resonances. This interferometric method is complemented by measurements on "metamaterial phase masks" (or metamaterial gratings) (Ref. 12) to experimentally determine the whole set of scattering parameters of the metafilm. A full electromagnetic finite-element model and an analytical two-layer model are used to analyze experimental results. The excellent agreement obtained between the two models, on the one hand, and that obtained between theoretical calculations and experimental measurements, on the other hand, allows us to retrieve the frequency evolution of the refractive index of the metamaterial around the first SRR resonance near normal incidence.

All metamaterial structures investigated in this work [Figs. 1(a)–1(c)] were fabricated on the same 280 μm thick, double-face polished silicon substrate using a single lithographic step. Structure (a) is the uniform metafilm made of gold nanowires and SRRs. Appropriate dimensions of these two familiar building blocks for metamaterials[13,14] are chosen to operate them in the infrared spectral range.[15] Structure (b) is a phase mask with alternated stripes of metamaterial and silicon. Structure (c) is the same as (b) except for the silicon stripes which are replaced by gold stripes. The entire fabrication process included e-beam lithography, e-beam evaporation of 5-nm-thick titanium, and 40-nm-thick gold films and a lift-off procedure. Patterning was achieved over 100 μm $\times$ 100 μm areas. The use of a single lithographic step allowed an accurate alignment of gold or silicon stripes with metamaterial motifs in the phase mask structures. It also ensured the reproducibility of metamaterial motifs from one patterned area to the other.

Two optical configurations were used to determine the metamaterial parameters in amplitude and in phase [Figs. 1(d) and 1(e)]. The novelty here lies in the comparative analysis of the Fabry-Perot-type cavities locally formed by patterned and unpatterned parts of the substrate, respectively

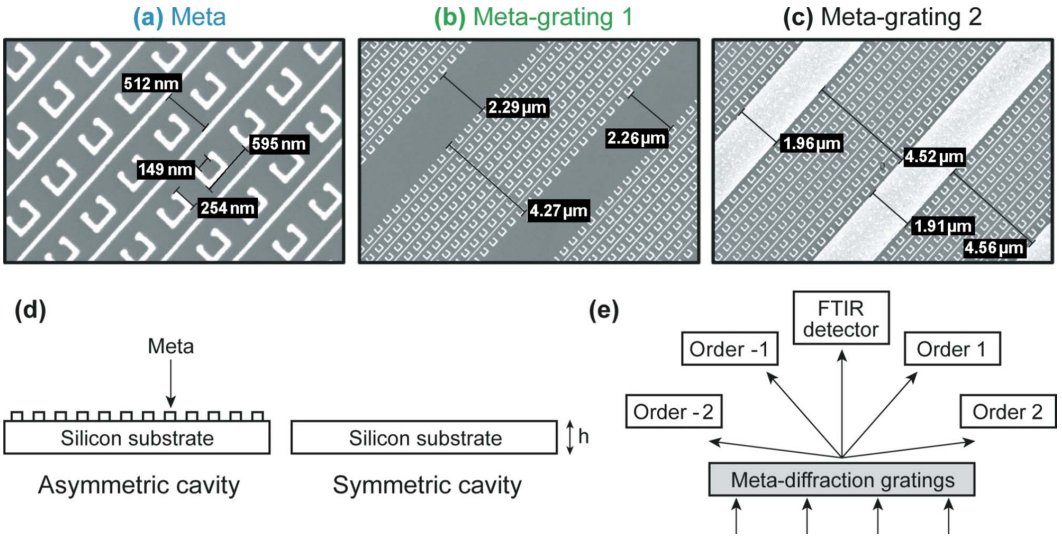

FIG. 1. (Color online) Top: electron micrographs of metamaterial structures, (a) uniform metafilm, (b) metafilm with silicon stripes, and (c) metafilm with gold stripes. Bottom: optical configurations investigated by Fourier transform infrared spectroscopy, (d) asymmetric cavity formed by a double-face polished silicon substrate and a uniform metafilm deposited on top-symmetric cavity simply formed by an unpatterned part of the same Si substrate. (e) Phase mask or diffraction metamaterial grating.

[Fig. 1(d)]. Patterned and unpatterned regions are chosen to be sufficiently close to each other in such a way that the small thickness variation throughout the double-face polished substrate has a negligible influence on the two cavity interferograms. In other words, the shift of interference fringes in one interferogram with respect to the other is only due to the presence (respectively, the absence) of metafilm on top of the substrate. Interferometric measurements on "phase masks" [Figs. 1(b) and 1(c)] are used to complete the phase information. Phase masks with alternated stripes of metamaterial and gold [Fig. 1(c)] are used to obtain the reflection phase at the air/metamaterial interface. Phase masks with alternated stripes of metamaterial and silicon [Fig. 1(b)] serve to estimate the phase shift after transmission through the metafilm. Figure 1(e) illustrates Fourier transform infrared (FTIR) measurements of the zero order of transmission in the case of the silicon/metamaterial phase mask.

Experimental measurements were performed near normal incidence with a Bio-Rad FTS 60A FTIR spectrometer equipped with a Cassegrain microscope. The FTIR beam was focused with a spot size smaller than 100 μm^2. The electric field of the incident light was polarized parallel to the SRR gap so as to couple SRR resonances with an odd number of electric nodes.[16] Electrical coupling to these SRRs resonances is of great interest for applications to nonmagnetic cloaking,[17] Epsilon near zero materials[18] and surface-enhanced Raman spectroscopy.[19] Figure 2(a) shows transmission spectra measured at low resolution on the three structures previously described in Figs. 1(a)–1(c). The transmission spectrum measured on the uniform metamaterial [blue curve in Fig. 2(a)] can be qualitatively seen as the superposition of the optical response of SRRs and of the Drude-type response associated to continuous nanowires.[13] The SRR resonance around 2400 cm^{-1} is the so-called *LC* resonance while the transmission dip detected around 5500 cm^{-1} corresponds to the second odd plasmonic mode. Transmission spectra measured for metagratings 1 and 2 [green and black curves in Fig. 2(a), respectively] exhibit the same overall shape. As expected, the transmission level is higher for metagrating 1 with silicon stripes than for metagrating 2 with gold stripes.

The second series of FTIR measurements was performed to resolve the Fabry-Perot resonances of both the symmetric cavity simply formed by double-face polished silicon [red curves in Figs. 2(b) and 2(c)] and the asymmetric cavity composed of the silicon substrate with the uniform metafilm on top [blue curves in Figs. 2(b) and 2(c)]. As seen in the high-resolution spectra of Fig. 2(b), the fringe contrast obtained in cavity measurements is small, which is explained by the ~30° FTIR beam divergence. Details on the relative positions of interference fringes for the two cavities are given in Fig. 2(c) around the LC resonance. The positions of maxima nearly coincide at 2020 cm^{-1} but a clear separation occurs at 2225 cm^{-1} and above. The amplitude maxima are shifted to higher frequencies in presence of the metafilm. The maximum shift is reached just below the SRR resonance with a value slightly smaller than half a cavity-free spectral range. Then a slow decrease is observed at larger frequencies (from 2380 to 2740 cm^{-1}). The evolution of the measured fringe shift is plotted versus wave number in Fig. 2(d) (black dots). Figure 2(d) also shows results of calculations from the two models used in our investigations. Thick continuous curves are numerical calculations from a finite-element code (HFSS from Ansoft) while thin curves are calculations from an analytical two-layer model. For each model, two different curves are shown which, respectively, correspond to two values of the damping frequency associated to the SRR resonant mode. In the full electromagnetic HFFS model, the permittivity and loss tangent of gold are simulated within the Drude approximation. The plasma frequency is fixed to: $\omega_p = 1.367 \times 10^{16}$ s^{-1} (f_p=2176 THz). The two collision (or damping) frequencies used in the calculations are ω_{c1}

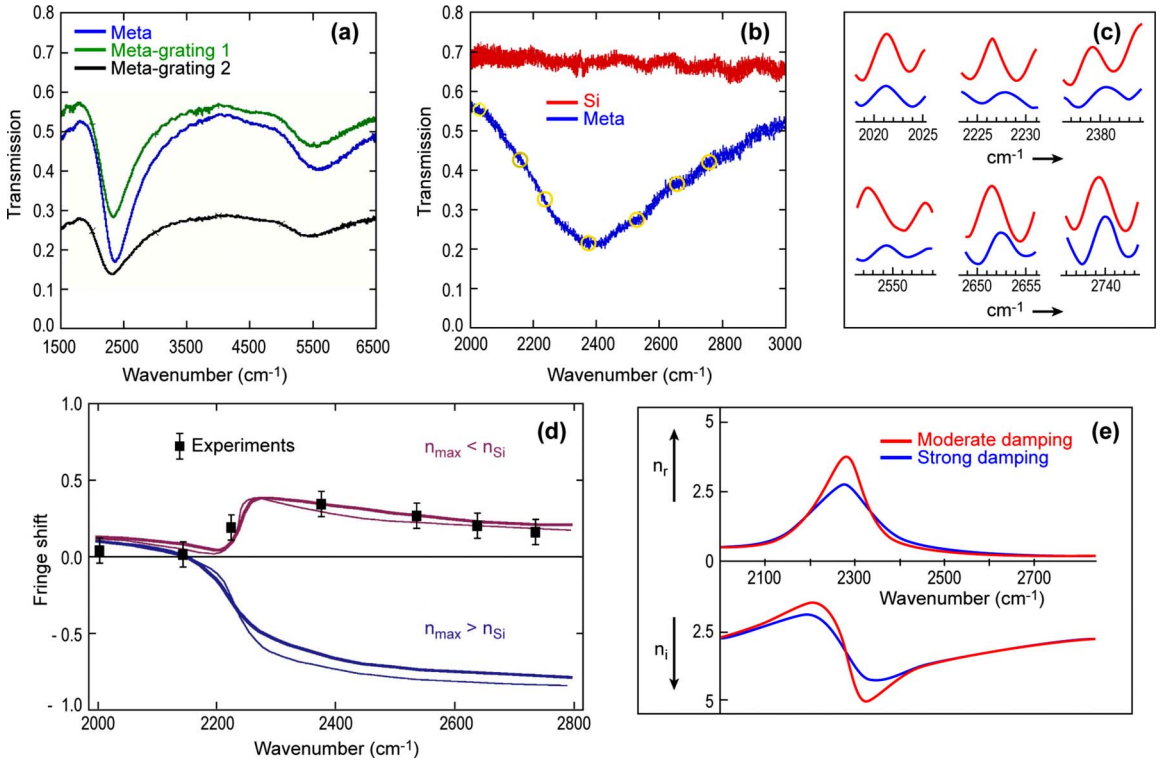

FIG. 2. (Color online) (a) Measured transmission spectra of metamaterial samples shown in Figs. 1(a)–1(c). (b) Measured interferograms of the symmetric (red) and asymmetric (blue) cavities shown in Fig. 1(d). (c) Details on respective fringe positions around the LC resonance [yellow circles in (b)]. (d) Fringe shift measured versus wave number (black dots) and calculations from finite-element model (thick curves) and two-layer model (thin curves). Two different values of damping frequencies are used in the models (see text). (e) Real and imaginary parts of the effective index of refraction calculated from the two-layer model for the two values of damping frequency.

$=6.478\times10^{13}$ s^{-1} ($f_{c1}=10.3$ THz) and $\omega_{c2}=1.5\omega_{c1}$ ($f_{c2}=15.45$ THz), respectively. Both values are significantly larger than in bulk gold, thus accounting for additional scattering experienced by electrons at metal surfaces. The first value is the same as that used in recent investigations of gold metafilms.[1,3,4,15] However, the fringe shift evolution calculated in this case [thick blue curve in Fig. 2(d)] is in total disagreement with experimental measurements: the amplitude maxima in the interferogram of the asymmetric cavity are shifted to low frequencies instead of high frequencies. Surprisingly, for damping frequencies ~1.4 larger than ω_{c1}, an abrupt transition occurs in the calculated phase behavior, and an excellent agreement is found between simulations and experiments for $\omega_c=\omega_{c2}$ [thick purple curve in Fig. 2(d)]. This dramatic change in phase behavior can be explained by the variation in the effective metamaterial index with damping frequency.

It is admittedly difficult to give rigorous analytical expressions of the effective parameters of an SRR medium since they depend on both the SRR shape and the dielectric environment.[20] Nevertheless, it has been shown that approximated expressions could be numerically derived even for asymmetric cells such as those used in our experiments:[21] for this purpose an averaged reflection coefficient was used for each interface in the retrieval procedure. However, only structural asymmetry but not substrate-induced asymmetry was considered in these simulations in the microwave domain. Moreover, the results have not been verified in experiments. Two simplifications can be exploited in our case. First, $\mu=1$ and $n=\sqrt{\varepsilon}$ since only the electric field couples to the metafilm near normal incidence. Second, high-order resonances can be neglected in the frequency domain of interest. Following that, the effective permittivity of the metafilm entering the two-layer model can be approximated as follows:

$$\varepsilon = 1 - \frac{\omega_{p,wires}^2}{\omega(\omega + i\omega_{c,wires})} - \frac{k}{(1-\omega_0^2/\omega^2) + i\omega_r\omega/\omega^2}. \quad (1)$$

The first terms in Eq. (1) synthesize the Drude-type response of the periodic array of continuous nanowires. For calculations, the plasma frequency was estimated from structure parameters:[13] $\omega_{p,wires}=1.3\times10^{15}$ s^{-1} ($f_{p,wires}\approx210$ THz) while the collision frequency $\omega_{c,wires}$ was varied in the range from ω_{c1} to ω_{c2}. It is worthwhile noticing that the choice of $\omega_{c,wires}$ had a relatively small influence on the results of calculations for the frequency domain of interest. The last term in Eq. (1) describes the LC resonance of SRRs. Following Onsager's principle, the expression is similar to the magnetic response originally derived in pioneering works on SRRs.[14] For calculations, the resonance frequency was taken in agreement with experimental measurements: $\omega_0=4.46\times10^{14}$ s^{-1} ($f_0\approx71$ THz). The k coefficient, which can be interpreted as an SRR filling factor,[14] was arbitrarily fixed equal to unity. The damping frequency was chosen to reproduce the measured linewidth of the resonant SRR mode [Fig. 2(b)]: $\omega_r\approx2.64\times10^{13}$ s^{-1} ($f_r\approx4.2$ THz). An "effective"

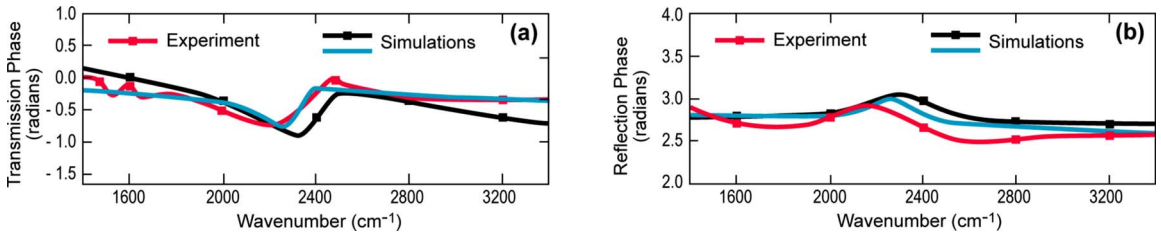

FIG. 3. (Color online) (a) Phase shift measured and simulated after transmission through the metafilm. (b) Reflection phase measured and simulated at the air/metafilm interface. In each case, red curves are measurements. Black and blue curves are simulations from the finite-element model and the two-layer model, respectively.

thickness of the metafilm, t, was also introduced to fit measured transmission levels with the two-layer model. The best fit was obtained for $t \approx 85$ nm, which is about two times larger than the thickness of the deposited layer. This discrepancy can be interpreted within the image theory applied to the metafilm on dielectric substrate.[22]

Using all the values of parameters listed above, a remarkable agreement is obtained between experimental results and the results of the two-layer model [thin purple curve in Fig. 2(d)]. Moreover, the entire interferogram of the asymmetric cavity (not shown here) is remarkably reproduced from analytical equations that can be solved with a pocket calculator. As previously predicted from the full electromagnetic model, modifying the collision/damping frequencies $\omega_{c,wires}$ and ω_r by a factor of 1.5 radically changes the phase behavior of the asymmetric cavity [thin blue curve in Fig. 2(d)]. An excellent agreement is thus also obtained between the two models. The phase behavior of the asymmetric cavity actually depends on the respective values of the metamaterial index at resonance and of the substrate index ($n_{Si} \approx 3.3$). Figure 2(e) shows the evolution of the effective metamaterial index (real and imaginary parts) calculated from Eq. (1) and $n = \sqrt{\varepsilon}$ for the two sets of collision/damping frequencies. Because of damping effects, the real part of the metamaterial index remains lower than the silicon index, and the transmission maxima of the asymmetric cavity are always in advance with respect to those of the symmetric cavity. These results implicitly show that disorder or imperfections[23] involved in metamaterial fabrication cannot only increase optical losses but also significantly alter the phase response of metafilms. It is worthwhile noticing that previous estimates of the damping frequency in infrared metamaterials based on gold nanostructures were exclusively derived from intensity measurements.[1,4,5] Cavity fringe (i.e., phase) measurements reported in this work represent a novel approach of quantifying scattering (i.e., dephasing) mechanisms for electrons in such nanostructures. Another result of major interest in Fig. 2(e) for applications such as optical cloaking[17] is the fact that the refractive index of the fabricated metafilm is predicted to vary in a wide range of values from ~0 to 3.

Transmission and reflection phases of the metafilm were investigated experimentally and numerically to further assess the validity of our models and interpretations. If T_{meta} is the power transmission of the metafilm, the complex transmission coefficient is expressed as: $t_{meta} = \sqrt{T_{meta}} e^{j\varphi_{meta}}$, where φ_{meta} is the unknown transmission phase. The latter can be deduced from the zero-order transmission of the phase mask sample [metagrating 1, Fig. 1(b)] which writes

$$T_{metagrating1} = |f_{1,1} t_{meta} + f_{2,1} t_{Si}|^2 = f_{1,1}^2 T_{meta} + f_{2,1}^2 T_{Si} + 2 f_{1,1} f_{2,1} \sqrt{T_{meta} T_{Si}} \cos(\varphi_{meta}), \quad (2)$$

where $f_{1,1}$ and $f_{2,1}$ are the relative fractions of metamaterial and silicon at the sample surface. T_{Si} and t_{Si} are the power and amplitude transmission of the unpatterned silicon substrate. Cavity effects are neglected for phase mask samples. Figure 3(a) shows the measured and calculated evolutions of the transmission phase with frequency. As is seen, the results confirm the excellent agreement between experiments and the models.

A similar procedure can be adopted for the reflection phase at the air/metafilm interface using the second phase mask [metagrating 2, Fig. 1(c)]. The only difference is that the phase shift measured at reflection includes the contribution of gold stripes. If R_{meta} is the power reflection of the metamaterial, the complex reflection coefficient is expressed as: $r_{meta} = \sqrt{R_{meta}} e^{j\phi_{meta}}$, where ϕ_{meta} is the reflection phase to be determined. In the same way, if R_{gold} is the power reflection of the reference gold mirror used in our experiments (a uniform gold layer deposited on silicon), the complex reflection coefficient r_{gold} can write: $r_{gold} = \sqrt{R_{gold}} e^{j\phi_{gold}}$, where the phase shift ϕ_{gold} is calculated from Drude relations applied to bulk gold. At this step, it is worthwhile mentioning that the value of damping frequency involved in Drude relations is typically 2–4 times smaller for bulk gold than for nanostructured gold.[1,4,5] Qualitatively, for any metallic film, the increase in the damping frequency with structuring is explained by the increase in the number of scattering events (collisions) experienced by electrons at the metal interfaces: The more pronounced the film structuring, the more probable the interface collisions. For bulk gold, the phase at reflection is close to π in the wave-number domain of investigation (below 3300 cm^{-1}). For the sake of simplicity, we presently take ϕ_{gold} equal to π. The phase term ϕ_{meta} is then deduced from the zero-order reflection of metagrating 2 using the following equation

$$R_{metagrating,2} = |f_{1,2} r_{meta} + f_{2,2} r_{gold}|^2 = f_{1,2}^2 R_{meta} + f_{2,2}^2 R_{gold} + 2 f_{1,2} f_{2,2} \sqrt{R_{meta} R_{gold}} \cos(\phi_{meta} + \phi_{gold}), \quad (3)$$

where $f_{1,2}$ and $f_{2,2}$ are the relative fractions of metamaterial and gold at the sample surface, and R_{gold} is determined from separate measurements on a gold layer on silicon. Results are reported in Fig. 3(b), which also confirms the general agreement between experiments and theoretical predictions. Some discrepancy between finite-element simulations (black curves) and results from Eqs. (2) and (3) (red curves) can be attributed to uncertainties in the geometrical parameters of SRRs estimated from scanning electron microscope images in Fig. 1.

At this stage, it is worthwhile mentioning that the asymmetric metafilm/silicon cavity cannot be simply described by a two-mirror model, where the phase difference per cavity roundtrip would be given by: $\delta=(4\pi/\lambda)n_{\mathrm{Si}}h+\phi(r_{meta/silicon})$ with λ, the wavelength, n_{Si}, the refractive index of silicon, h, the cavity height, and $\phi(r_{meta/silicon})$, the reflection phase at the metafilm/silicon interface. Indeed, calculations of the cavity resonances from $\delta=2k\pi$ with k integer led to fringe shift evolutions, which radically differed from those reported in Fig. 2(d). The correct analytical description of a metafilm on a dielectric substrate must treat the metafilm as a whole layer with effective parameters and two interfaces.

In conclusion, we have experimentally and theoretically demonstrated that a thin metafilm deposited on a dielectric substrate can be consistently described within the effective-index approach. This demonstration is based on the excellent agreement between experiments, a two-layer analytical model and a full electromagnetic model of the asymmetric metafilm/substrate system. A detailed interferometric analysis, in amplitude and in phase (using Fabry-Perot cavities and phase samples) of a metafilm composed of metallic nanowires and split ring nanoresonators on silicon has been reported. Results show that contrary to intensity transmission/reflection characteristics, the phase behavior of an air/metafilm/dielectric system may critically depend on the damping frequency associated to plasmonic resonances, which itself depends on scattering experienced by electrons in the material as well as on structure disorder. This work represents an important step toward the understanding of optical properties of composite metamaterials especially in the case where they are combined with dielectric layers or substrate of high permittivity. Models and experimental methods presently developed for normal incidence can be potentially adapted to more complex situations where metafilms are illuminated at oblique or grazing incidence. This perspective would be of great interest for future metamaterial-based devices in guided optics.

The authors thank F. Gadot for fruitful discussions. This work has been supported by the French Research Agency through the METAPHOTONIQUE project.

*boubacar.kante@ief.u-psud.fr
†jean-michel.lourtioz@ief.u-psud.fr

[1] S. Linden, C. Enkrich, M. Wegener, J. Zhou, T. Koschny, and C. M. Soukoulis, Science **306**, 1351 (2004).
[2] V. M. Shalaev, W. Cai, U. K. Chettiar, H. K. Yuan, A. K. Sarychev, V. P. Drachev, and A. V. Kildishev, Opt. Lett. **30**, 3356 (2005).
[3] G. Dolling, C. Enkrich, M. Wegener, C. M. Soukoulis, and S. Linden, Science **312**, 892 (2006).
[4] N. Liu, H. Guo, L. Fu, S. Kaiser, H. Schweizer, and H. Giessen, Nature Mater. **7**, 31 (2008).
[5] J. Valentine, S. Zhang, T. Zentgraf, E. U. Avila, D. A. Genov, G. Bartal, and X. Zhang, Nature (London) **455**, 376 (2008).
[6] A. M. Nicolson and G. F. Ross, IEEE Trans. Instrum. Meas. **19**, 377 (1970).
[7] W. B. Weir, Proc. IEEE **62**, 33 (1974).
[8] D. R. Smith, S. Schultz, P. Markos, and C. M. Soukoulis, Phys. Rev. B **65**, 195104 (2002).
[9] A. Pinchuk, A. Hilger, G. von Plessen, and U. Kreibig, Nanotechnology **15**, 1890 (2004).
[10] A. Curry, G. Nusz, A. Chilkoti, and A. Wax, Opt. Express **13**, 2668 (2005).
[11] C. Rockstuhl, T. Paul, F. Lederer, T. Pertsch, T. Zentgraf, T. P. Meyrath, and H. Giessen, Phys. Rev. B **77**, 035126 (2008).
[12] S. Zhang, W. Fan, N. C. Panoiu, K. J. Malloy, R. M. Osgood, and S. R. J. Brueck, Phys. Rev. Lett. **95**, 137404 (2005).
[13] J. B. Pendry, A. J. Holden, D. J. Robbins, and W. J. Stewart, J. Phys.: Condens. Matter **10**, 4785 (1998).
[14] J. B. Pendry, A. J. Holden, D. J. Robbins, and W. J. Stewart, IEEE Trans. Microwave Theory Tech. **47**, 2075 (1999).
[15] B. Kanté, A. de Lustrac, J.-M. Lourtioz, and F. Gadot, Opt. Express **16**, 6774 (2008).
[16] C. Rockstuhl, F. Lederer, C. Etrich, T. Zentgraf, J. Kuhl, and H. Giessen, Opt. Express **14**, 8827 (2006).
[17] B. Kanté, A. de Lustrac, J.-M. Lourtioz, and S. N. Burokur, Opt. Express **16**, 9191 (2008).
[18] A. Alù, M. G. Silveirinha, A. Salandrino, and N. Engheta, Phys. Rev. B **75**, 155410 (2007).
[19] B. Kanté, A. de Lustrac, and J. M. Lourtioz, Phys. Rev. B **80**, 035108 (2009).
[20] R. Marqués, F. Medina, and R. Rafii-El-Idrissi, Phys. Rev. B **65**, 144440 (2002).
[21] D. R. Smith, D. C. Vier, Th. Koschny, and C. M. Soukoulis, Phys. Rev. E **71**, 036617 (2005).
[22] M. K. Knight, Y. Wu, J. B. Lassiter, P. Nordlander, and N. J. Halas, Nano Lett. **9**, 2188 (2009).
[23] M. Gorkunov, S. A. Gredeskul, I. V. Shadrivov, and Y. S. Kivshar, Phys. Rev. E **73**, 056605 (2006).